Super-X: A Soft X-ray Telescope for *Solar-B*

Loren Acton[a], Jay Bookbinder[b], Marilyn Bruner[c], Leon Golub[b], and James Lemen[c]

[a]Physics Dept., Montana State University, Bozeman, MT 59771, USA

[b]Harvard-Smithsonian Center for Astrophysics
60 Garden St. MS-58, Cambridge, MA 02138, USA

[c]Solar & Astrophysics Laboratory
Lockheed Martin Advanced Technology Center
Bldg. 252, Org. H1-12, 3251 Hanover Street, Palo Alto, CA 94304, USA

ABSTRACT

This paper describes the conceptual design of a soft X-ray telescope, Super-X, which we will propose for the Japan/US/UK *Solar-B* mission. Super-X will break new ground in both angular resolution and solar coronal temperature discrimination. The telescope design is based upon the successful *Transition Region and Coronal Explorer* instrument. It features four XUV spectral channels spanning the 0.3 to 30 MK temperature range with an angular resoluton of approximately 0.27 seconds of arc. We will describe considerations affecting spectral line selection and some details of the characteristics of the instrument.

Keywords: Solar-B, X-ray, telescope, sun, multilayer optics, corona

1. INTRODUCTION

Solar-B is a mission of the Institute of Space and Astronautical Science in Japan with cooperation by the National Aeronautics and Space Administration in the USA. and the Particle Physics and Astronomy Research Council in the UK. Its purpose is to enable an improved understanding of the magnetic processes which are believed to be the energy source of all manifestations of solar activity. *Solar-B* will build upon previous, very successful, ISAS solar missions, *Hinotori*[1] and *Yohkoh*,[2] the *Solar and Heliospheric Observatory*[3] (*SOHO*) of ESA and NASA, and the *Transition Region and Coronal Explorer*[4,5] (*TRACE*) – a NASA small explorer mission launched in April 1998. *Solar-B* is scheduled for launch into a polar, full sun, orbit from ISAS's Kagoshima Space Station in February 2004.

The primary scientific instrument on *Solar-B* is a half-meter diffraction-limited optical Gregorian telescope. This telescope feeds a focal plane package, to be provided by NASA, for the purpose of narrow-band imagery and magnetography. *Solar-B* will provide the first space vector measurements of the magnetic fields in the sun's photosphere with a sensitivity of about 8 and 60 gauss, respectively, for the longitudinal and transverse components of the field. The angular resolution of the optical telescope will be 0.2 seconds of arc. Further details of the scientific objectives of the mission and the strawman payload are given in *The Solar-B Mission: Final Report of the Science Definition Team (SDT)* which may be found on the World Wide Web at http://wwwssl.msfc.nasa.gov/ssl/pad/solar/sdt-rpt.htm.

To achieve the scientific objectives of the *Solar-B* mission it is necessary to obtain observations in higher layers of the atmosphere, where it is postulated that magnetic energy is released to provide the many manifestations of the active sun. The two auxiliary instruments included in the strawman payload for this purpose are the Extreme-ultraviolet Imaging Spectrometer (EIS), to be provided by a cooperation involving the USA, the UK, and Japan, and the Soft X-ray Telescope.

It is the purpose of this paper to describe Super-X, our proposal for the *Solar-B* Soft X-ray Telescope. Super-X is a 4-channel reflecting multilayer telescope similar in design concept to the Extreme-ultraviolet Imaging Telescope

Other author information: (Send correspondence to L. A.)
L.A.: E-mail: acton@physics.montana.edu
J.B.: E-mail: bookbind@head-cfa.harvard.edu
M.B.: E-mail: bruner@lmsal.com
L.G.: E-mail: golub@kodos.harvard.edu
J.L.: E-mail: lemen@lmsal.com

(EIT) on *SOHO* and the *TRACE* instrument. Super-X will provide higher angular resolution than either EIT or *TRACE*. Furthermore, the coronal temperature response of the four Super-X channels will be specifically tailored to the requirements of *Solar-B* science. In the following section we discuss the selection of X-ray emission lines to be imaged by Super-X. Following this we will briefly describe our proposed design and the technical characteristics of the instrument.

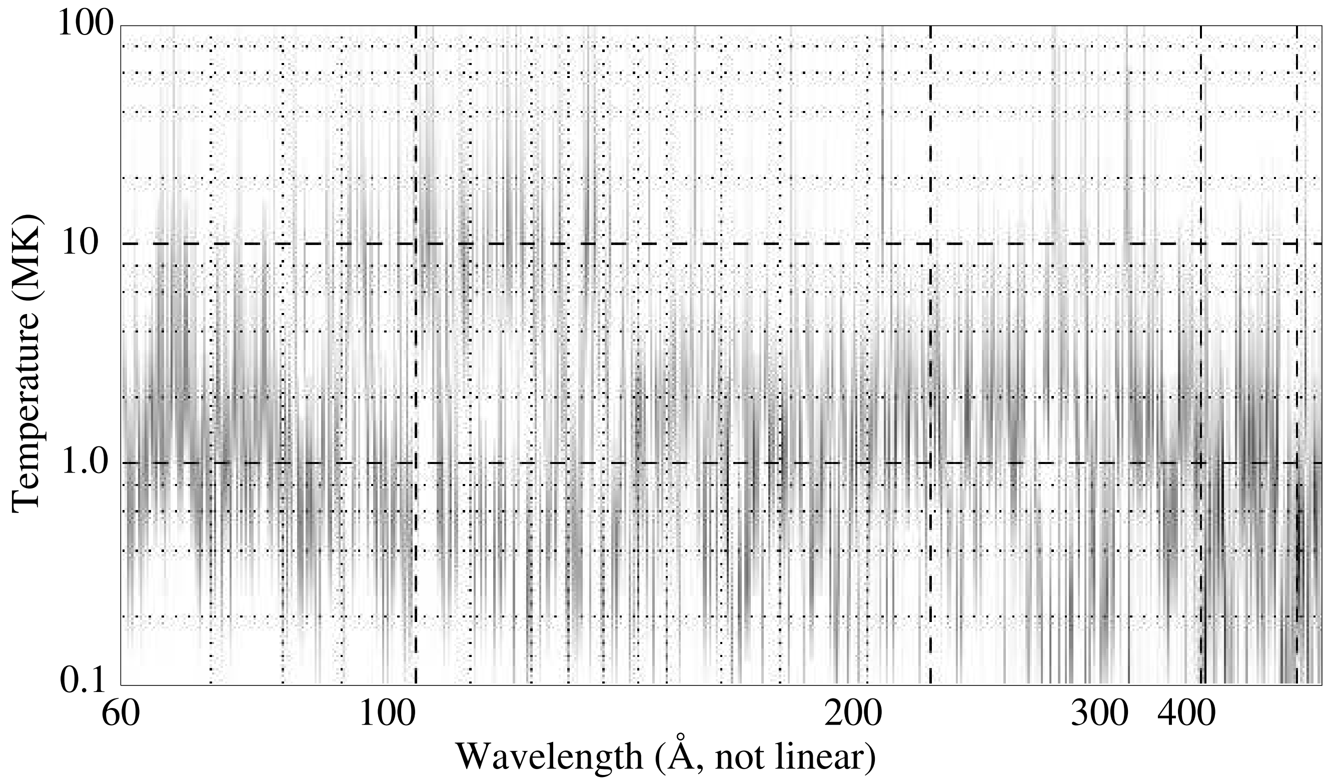

Figure 1. Theoretical solar emission line spectrum from 60-440 Å. Each vertical mark represents a line. The vertical extent reflects the temperature range over which the line appears as shown by the vertical logarithmic temperature scale. Line strength on a log scale is crudely indicated by the darkness of the mark. The wavelength scale is non-linear in order to display the entire spectrum on one figure. For clarity, no 10 Å markers are plotted beyond 200 Å.

2. SELECTION OF X-RAY EMISSION LINES FOR SUPER-X

The choice of spectral response of the four Super-X channels is constrained by the strength and temperature response of the emission lines available in the solar soft X-ray spectrum as well as the optical properties of transmission filters, multilayer mirrors, and the CCD. In this section we examine alternatives and describe software tools developed to facilitate our survey of the possibilities.

2.1. The Soft X-ray Spectrum

Our analysis employs the analytical model of the soft X-ray emission from an optically-thin equilibrium plasma of Mewe, *et al.*.[6,7] The ionization balance values of Arnaud and Raymond[8] are utilized for iron and of Arnaud and Rothenflug[9] for all other elements. Solar coronal elemental abundances are after Meyer.[10] We have examined the entire 60-410 Å spectral interval—a region rich in coronal emission lines and where we are confident of the ability to procure usable multilayer optics.

Mewe's model lists 1100 emission lines in the 60-440 Å interval, with peak temperatures ranging from below 0.1 to above 10 MK. The nature of the emission line spectrum through this interval is illustrated in Fig. 1.

2.2. Super-X Response

The CCD signal in electrons from an observation by a multilayer telescope such as Super-X is given by Equation (1).

$$S_{\lambda_0}{=}ABCE\int_{\lambda}G_1(\lambda)R_p(\lambda,\lambda_0)R_s(\lambda,\lambda_0)G_2(\lambda)D(\lambda)\int_V N_e{}^2(T_V)F(\lambda,T_V)dVd\lambda. \tag{1}$$

The variables in this equation are defined as follows.

S	=	CCD signal for a multilayer centered at wavelength λ_0 (electrons),
λ_0	=	Wavelength of peak multilayer reflectivity,
A	=	Geometrical area (160 cm^2),
B	=	$(4\pi\times\mathrm{AU}^2)^{-1} = 3.5\times10^{-28}\mathrm{cm}^{-2}$,
C	=	Conversion constant (1.71×10^{11}electrons erg^{-1}),
E	=	Exposure time (sec),
G	=	Entrance and rear filter transmission,
R	=	Primary and secondary multilayer mirror reflectivity,
D	=	Quantum efficiency of the CCD,
N_e	=	Electron density (cm^{-3}),
F	=	Solar emissivity from Mewe *et al.*[6,7] *(erg cm^3 s^{-1})*,
V	=	Volume of the observed solar feature (cm^{-3}).

The geometrical aperture, A, corresponds to one quadrant of the 30 cm diameter primary mirror – after allowing for obscuration by structure and the secondary mirror. The integral over volume is effectively an integral over temperature and differential emission measure, $N_e{}^2(T_V)\times dV$.

A solar X-ray telescope requires optically opaque filters in the optical path to exclude the vastly dominant longer wavelengths from the image plane. Thin metal foils, appropriately transmissive at the desired X-ray wavelengths, are typically employed for this purpose. As entrance filters are subject to piercing in orbit by micrometeorites, opening pinholes which leak light, the Super-X design incorporates secondary filters of the same material in filter wheels—directly in front of the shutter.

Our design analysis is based on the use of 1500 Å zirconium filters for wavelengths below the aluminum L-edge at 171 Å and 1500 Å aluminum for longer wavelengths. The filters are supported on either 1000 Å polyimide or 28 line/cm nickel mesh (80% transmission). The polyimide support material has the advantage of freedom from diffraction effects, but becomes less transmissive than the mesh for wavelengths longer than about 110 Å. Zr filters on both polyimide and mesh have been successfully fabricated by Luxel^{TM} and tested in our laboratory.

The Zr entrance filter on polyimide transmits enough visible light ($\sim 10^{-5}$) to permit forming an image of the solar photosphere on the CCD with an appropriate optical filter in the aft filter wheel. This will be utilized for pointing and co-alignment as described in section 3 below.

The Super-X detector is a thinned, back-illuminated, 2048×2048 CCD with 13.5 μm pixels, produced by English Electric Valve (EEV) in the UK. The calculated quantum efficiency (QE) of these CCDs is greater than 0.6 throughout the 60-410 Å region. Laboratory tests on a similar EEV device are presently underway at Lockheed Martin to confirm QE and quantify resistance to radiation damage engendered by the EEV production processes.

2.3. Multilayer Reflectivity

The use of normal incidence multilayer mirrors for EUV and X-ray imaging in space is, if not routine, at least a mature technology. However, designing a multilayer mirror for every wavelength from 60-410 Å is too tedious for a rapid survey of instrument design possibilities. Thus, we have taken the tack of fitting analytic functions to the parameters of Voigt functions fit to 9 multilayers spanning this spectral interval. These were either computed from the optical constants of appropriate materials or taken from laboratory measurements of multilayer mirrors. For any given mirror the Voigt function fits the profile quite adequately. The model mirrors derived from our parametric fits are less good – but very convenient for computation and good enough for our purposes.

The IDL^{TM} programs used to compute the Voigt function expression for a multilayer reflectivity are given in the appendix. Fig. 2 illustrates the quality of the reflectivity match between the 9 mirrors and our analytic functions.

2.4. Baseline Wavelengths for Super-X

The solution of equation (1) for all wavelengths 60–410 Å and for all (isothermal) coronal temperatures between 0.1 and 100 MK is depicted in Fig. 3. A vertical cut across the floating point version of this temperature-wavelength array yields the approximate temperature response of Super-X for a channel prepared for that wavelength. An interactive IDL^{TM} program has been prepared by which a click on the figure returns the approximate Super-X temperature response for a multilayer at that wavelength.

High resolution imaging requires a reasonably strong signal in each spectral range. Therefore, only stronger emission lines are chosen at wavelengths where high reflectivity multilayer optics can be made. In addition, wavelengths with a fairly "clean" temperature response are desirable, as are spectral channels that allow temperature diagnostics by means of intensity ratios. The use of lines of a single element (Fe) is preferred, although not always possible, in order to avoid difficulties of interpretation related to possible variation in elemental abundances.

A study of Fig. 3 shows that there are limited possibilities for choosing strong lines that sample a narrow and cleanly defined temperature range. The most interesting candidates are listed in Table 1 where the units of Super-X signal are electrons s^{-1} per 10^{44} cm^{-3} emission measure at the given temperature. We have listed the dominant transitions in each case.

Although most of these wavelengths provide a response to a narrow, well-isolated temperature range they all blend several emission lines of various strengths. The 119 Å line is an interesting special case with 2 cleanly defined response peaks widely separated at 0.27 and 8 MK.

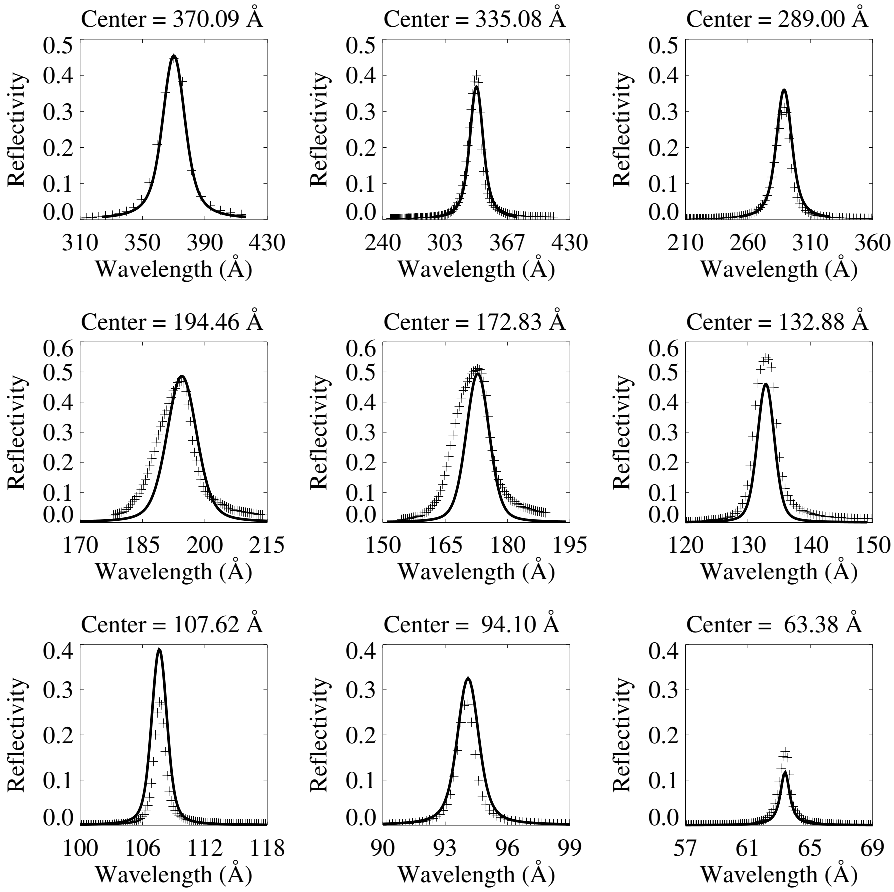

Figure 2. Comparison of input multilayer reflectivity profiles (crosses) and profiles computed with voigt_refl.pro (solid line), given in Appendix A.

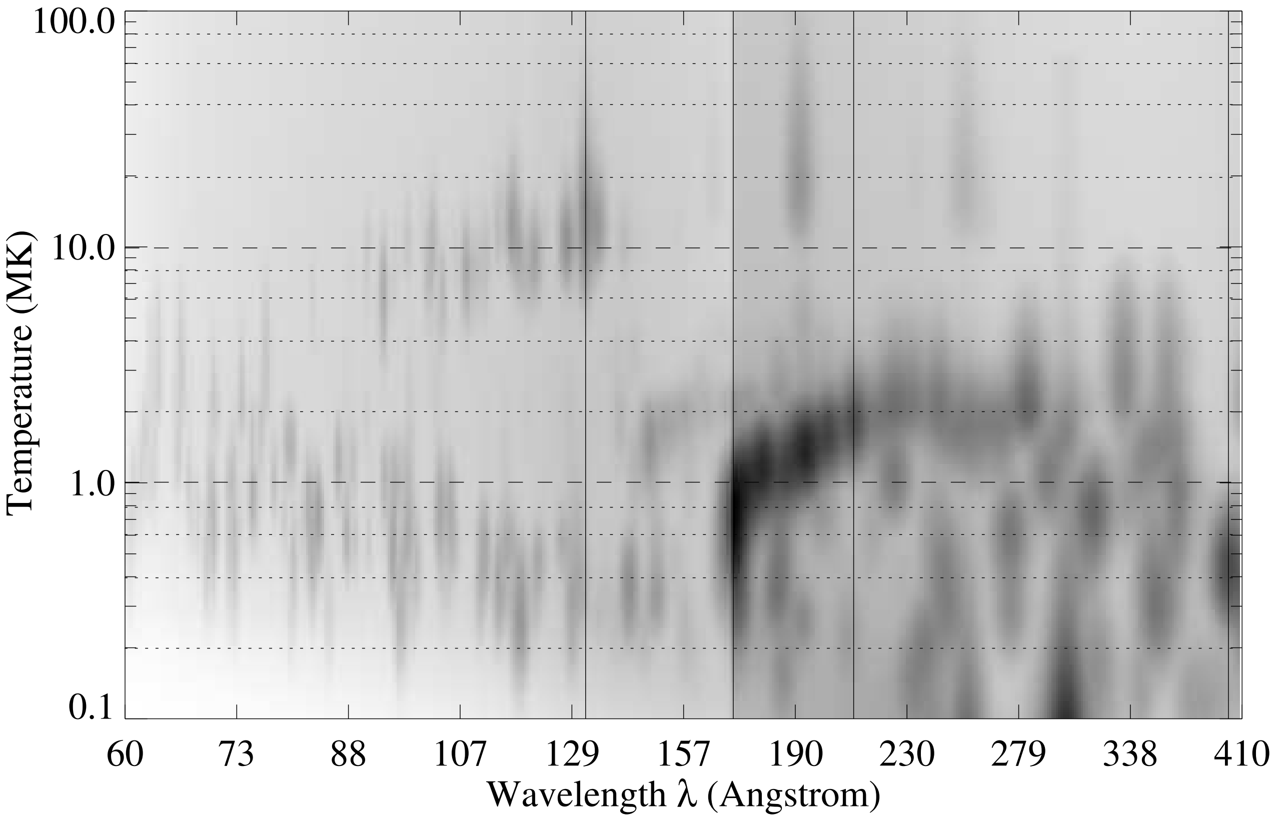

Figure 3. The approximate temperature response of Super-X for a multilayer mirror tuned to wavelength λ. The gray scale represents CCD signal in units of electrons sec^{-1} for an emission measure of 10^{44} cm^{-3}. The minimum (white) and maximum(black) values in these units range from 1.3×10^{-6} to $1.5 \times 10^{+6}$, respectively. The response discontinuity at 171 Å relates to the aluminum L-edge of the filters. Vertical lines at 133, 171, 211, and 400 Å indicate the positions of the four baseline Super-X channels.

We have tentatively selected the following wavelengths as the baseline set for Super-X. The final selection will be made in consultation with the *Solar-B* Science Working Group during the *Solar-B* Phase A study.

400 Å – Mg VI & Ne VI : This is the brightest and cleanest 0.5 MK channel in the EUV, and allows imaging of the low temperature corona / transition region with reasonable exposure times. No suitable Fe lines are available in that temperature range. This channel employs an VSi_2/Mg_2Si multilayer which is new to U.S. manufacturers but has been made in Russia.[11] An alternative line, Ne V at 142.7 Å does not require multilayer development – but is somewhat lower in temperature and weaker than the 400 Å feature.

171 Å – Fe IX-X : This is the lowest temperature Fe channel that fulfills the criteria of being bright, clean, and technically feasible. In addition, it is a *TRACE* favorite. The multilayer is Si/Mo.

211 Å – Fe XIV : This channel is intended to show the higher temperature component of the solar minimum corona. It has been used on a rocket instrument[12] with excellent results. The images look very much like the thin-filter images from the *Yohkoh* Soft X-ray Telescope. It is particularly clean and brighter than the alternative 284 Å - Fe XV channel. The multilayer is $MoSi_2/S$.

133 Å – Fe XX-XXIII : This channel is dedicated to the observation of transient heating events in the 5-20 MK range. The 133 Å channel peaks at about 11 MK, is fairly bright and responds to a broad range of high temperatures. Lastly, the 133 Å entrance filter will be meshless (1500 Å Zr + 1000 Å polyimide) and suitable for visible light imaging. The multilayer is Si/Mo.

Table 1. Candidate Emission Lines for Super-X

Wavelength (Å)	Principal Ion	Super-X Signal	Peak Temp (K)
93.9	Fe XVIII	5×10^3	6.3×10^6
	Fe X	3×10^3	1.0×10^6
108.4	Fe XIX	5×10^3	7.7×10^6
119.0	Si V	2×10^4	2.7×10^5
	Fe XX	6×10^3	8.9×10^6
132.9	Fe XXIII	3×10^4	1.3×10^7
142.7	Ne V	2×10^4	3.6×10^5
171.1	Fe IX	7×10^5	7.2×10^5
177.2	Fe X	3×10^5	9.8×10^5
180.3	Fe XI	3×10^5	1.2×10^6
193.5	Fe XII	4×10^5	1.4×10^6
202.0	Fe XIII	2×10^5	1.6×10^6
211.3	Fe XIV	1×10^5	1.9×10^6
284.2	Fe XV	6×10^4	2.1×10^6
319.0	Mg VII	4×10^5	6.4×10^5
353.1	Mg V	4×10^4	2.9×10^5
401.6	Ne VI	1×10^5	4.4×10^5

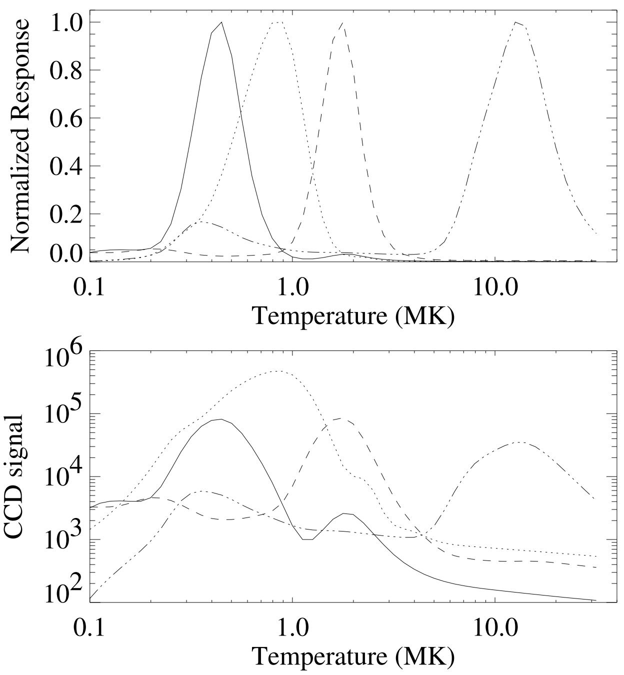

Figure 4. Temperature response of the baseline Super-X. The units of CCD Signal are electrons s^{-1} for an emission measure of 10^{44} cm^{-3}.

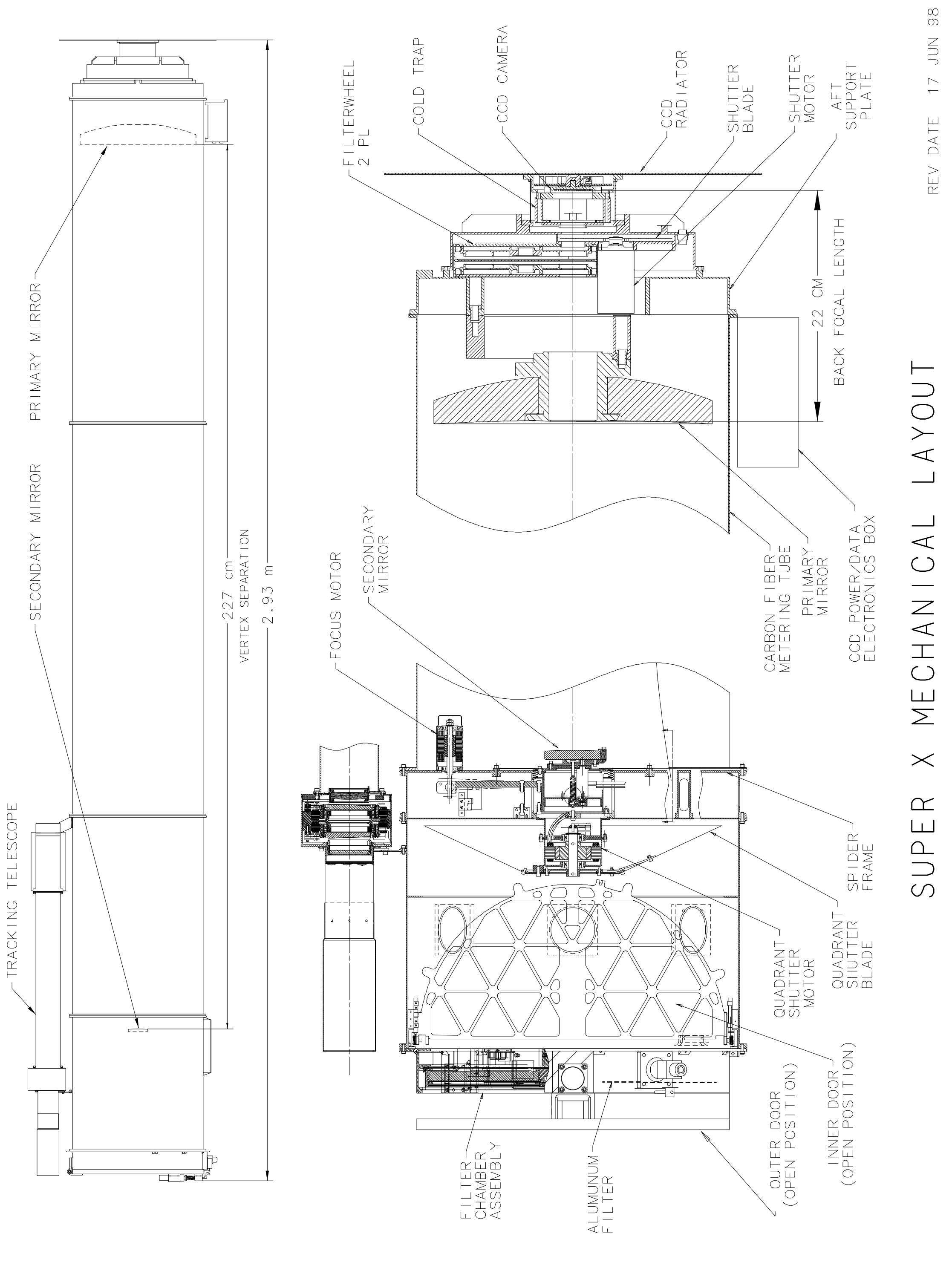

Figure 5. Schematic illustration of Super-X, based on TRACE drawings. Dimensions are correct but some details will be changed.

Figure 4 illustrates the temperature response and sensitivity of the baseline Super-X spectral channels. These response curves were prepared from actual or computed multilayer reflectivity curves, not from the analytical approximation used in our survey work.

3. SUPER-X DESIGN

The Super-X instrument borrows heavily from the very successful *TRACE*[4,5] multilayer telescope. It is a Cassegrain reflector with the design parameters as shown in Table 2. Anyone interested in further information about the *TRACE* instrument or viewing some of the spectacular solar images and movies are invited to visit the *TRACE* URL at http://vestige.lmsal.com/TRACE/TRACElinks.html.

Table 2. Super-X Design Parameters

Primary Diameter	30.0 cm
Magnification	8.0
Primary focal length	258.0 cm
Primary focal ratio	8.6
Eff. focal length	2064.4 cm
Eff. focal ratio	68.8
Pixel size	13.5 μm
Pixel subtense	0.135 arcsec
Overall Length	300.0 cm
Number of pixels	2048×2048
Field size	276 arcsec

An active tip-tilt secondary mirror assembly on Super-X will provide for focus adjustment and image motion compensation (IMC). The IMC error signal will be provided by solar limb sensors on the attached tracking telescope. Images taken in visible light through the 133 Å channel will be cross-correlated with granulation pictures from the *Solar-B* optical telescope to provide scene co-alignment between the two instruments to a fraction of a pixel. As high precision co-alignment is crucial to the scientific success of *Solar-B* we will consider in Phase A whether this cross-correlation will be done as part of data analysis or should be done on board. In the latter case it could be used to generate bias signals to the Super-X active secondary to keep the two fields of view congruent despite solar rotation and possible pointing drifts within either of the instruments.

Figure 5 illustrates the main features of our preliminary design for Super-X. If selected, we expect that some details will change during Phase A and that some elements of the telescope and/or the control and data processing electronics will be provided by our Japanese colleagues.

APPENDIX A. IDL^{TM} CODES FOR MULTILAYER MIRRORS

The IDL^{TM} program voigt_refl.pro.

```
voigt_refl,wave,refl,ll,dwave=dwave

;+
; NAME
;       voigt_refl
; PURPOSE
;       Compute multi-layer reflectivity for arbitrary wavelength between
;       94 and 400 A based upon voigt fits to Golub reflectivity data.
; METHOD
;       Use semi-log polynomial fits to the voigt reflectivity parameters
;       for 370.090, 335.081, 288.998, 194.460, 172.828, 132.883,
;       107.622, 94.0953, 63.3845 angstroms.
```

```
; CALLING SEQUENCE
;       voigt_refl,wave,refl,ll [,dave=dwave]
; INPUT
;       wave, central wavelength of desired reflectivity peak (Angstrom).
; OPTIONAL KEYWORD INPUT
;       dwave, half width of output spectral interval in Angstrom.
;       Default is wave/8.
; OUTPUT
;       refl = reflectivity vs. wavelength
;       ll   = wavelength array, centered on wave, n_elements = 200.
; PROGRAMS CALLED
;       mvoigt.pro
; HISTORY
;       3/17/98 LWA
;       3/19/98 LWA, Changed voigt profile resolution to 0.1 A.
;       4/27/98 LWA, Recomputed voigt fit parameters.
;       6/24/98 LWA, Assured wave was floating point.
;-

wave=float(wave)
f3 = [-2.76343, 0.0370483, -0.000128409, 1.51115e-07]
f5 = [-2.61139, 0.0349961, -0.000121998, 1.42007e-07]
f6 = [0.445820, -0.0272144, 0.000233073, -6.33308e-07, 5.59238e-10]
aa=[0,0,0,$
    10^(f3(0)+f3(1)*wave+f3(2)*wave^2+f3(3)*wave^3), wave,$
    10^(f5(0)+f5(1)*wave+f5(2)*wave^2+f5(3)*wave^3),$
    10^(f6(0)+f6(1)*wave+f6(2)*wave^2+f6(3)*wave^3+f6(4)*wave^4)]
if NOT keyword_set(dwave) then dwave=wave/8. else dwave=dwave
ll=round(wave-dwave)+.1*findgen(dwave*2/.1)
refl=mvoigt(ll,aa)

end
```

The IDL^{TM} program mvoigt.pro is included in the SolarSoft data analysis software system and may be obtained through the URL http://www.lmsal.com/solarsoft/.

ACKNOWLEDGMENTS

We extend our hearty thanks to Japanese, American and British colleagues who are bringing the *Solar-B* mission to fruition.

REFERENCES

1. K. Tanaka, "Impact of x-ray observations from the hinotori satellite on solar flare research," *Publ. Astron. Soc. Japan* **39**, pp. 1–45, 1987.
2. Y. Ogawara, T. Takano, T. Kato, T. Kosugi, S. Tsuneta, T. Watanabe, I. Kondo, and Y. Uchida, "The solar-a mission: an overview," *Solar Physics* **136**, pp. 1–16, 1991.
3. V. Domingo, B. Fleck, and A. I. Poland, "The soho mission: An overview," *Solar Physics* **162**, pp. 1–37, 1995.
4. T. D. Tarbell, M. Bruner, B. Jurcevich, J. Lemen, K. Strong, A. Title, J. Wolfson, L. Golub, and R. Fisher, "The transition region and coronal explorer (trace)," in *Proc. of the Third SoHO Workshop — Solar Dynamic Phenomena and Solar Wind Consequences 26–29 September 1994*, p. 375, 1994.
5. B. N. Handy, M. E. Bruner, T. D. Tarbell, A. M. Title, and C. J. Wolfson, "Uv observations with the *Transition Region and Coronal Explorer*," *Solar Physics* **in press**, 1998.
6. R. Mewe, E. H. B. M. Gronenschild, and G. H. J. van den Oord, "Calculated x-radiation from optically thin plasmas. v.," *Astron. & Astrophys. Suppl.* **62**, pp. 197–254, 1985.

7. R. Mewe, J. R. Lemen, and G. H. J. van den Oord, "Calculated x-radiation from optically thin plasmas. vi.," *Astron. & Astrophys. Suppl.* **65**, pp. 511–536, 1986.
8. M. Arnaud and J. Raymond, "Iron ionization and recomination rates and ionization equilibrium," *Astrophys. J.* **398**, pp. 394–406, 1992.
9. M. Arnaud and R. Rothenflug, "An updated evaluation of recombination and ionization rates," *Astron. & Astrophys. Suppl.* **60**, pp. 425–457, 1985.
10. J.-P. Meyer, "Solar-stellar outer atmospheres and energetic particles, and galactic cosmic rays," *Astrophys. J. Suppl.* **57**, pp. 173–204, 1985.
11. Y. A. Uspenskii, V. E. Levashov, A. V. Vinogradov, A. I. Fedorenko, and et al., "High-reflectivity multilayer mirrors for a vacuum- ultraviolet interval of 35-50 nm," *Optics Letter* **23**, p. 771, 1998.
12. H. Hara, R. Kano, S. Nagata, T. Sakao, T. Shimizu, S. Tsuneta, T. Yoshida, and T. Kosugi, "Xuv doppler telescope with multilayer optics," *Proc. SPIE* **3113**, pp. 420–429, 1997.